

Class I methanol masers in low-mass star formation regions

S. Kalenskii¹, S. Kurtz², P. Hofner³, P. Bergman⁴, C.M. Walmsley⁵,
and P. Golysheva⁶

¹Lebedev Physical Institute, Astro Space Center,
84/32 Profsoyuznaya st., Moscow, GSP-7, 117997, Russia
email: kalensky@asc.rssi.ru

²Instituto de Radioastronomia y Astrofísica, Universidad Nacional Autónoma de México,
Morelia, Michoacán, México
email: s.kurtz@irya.unam.mx

³National Radio Astronomy Observatory, 1003 Lopezville Road, Socorro, NM 87801, USA
email: hofner_p@yahoo.com

⁴Onsala Space Observatory, Chalmers Univ. of Technology, 439 92 Onsala, Sweden
email: per.bergman@chalmers.se

⁵Dublin Institute for Advanced Studies, 31 Fitzwilliam Place, Dublin 2, Ireland (deceased)

⁶119992, Universitetski pr., 13, Sternberg Astronomical Institute, Moscow University, Moscow,
Russia
email: polina-golysheva@yandex.ru

Abstract. We present a review of the properties of Class I methanol masers detected in low-mass star forming regions (LMSFRs). These masers, henceforth called LMMIs, are associated with postshock gas in the lobes of chemically active outflows in LMSFRs NGC1333, NGC2023, HH25, and L1157. LMMIs share the main properties with powerful masers in regions of massive star formation and are a low-luminosity edge of the total Class I maser population. However, the exploration of just these objects may push forward the exploration of Class I masers, since many LMSFRs are located only 200–300 pc from the Sun, making it possible to study associated objects in detail. EVLA observations with a 0.2'' spatial resolution show that the maser images consist of unresolved or barely resolved spots with brightness temperatures up to 5×10^5 K. The results are "marginally" consistent with the turbulent model of maser emission.

Keywords. ISM: jets and outflows, masers, radio lines: ISM.

1. Introduction

Bright and narrow maser lines of methanol (CH_3OH) have been found towards many star-forming regions. Methanol masers can be divided into two classes, I and II (Menten, 1991b), with each class characterized by a certain set of transitions. Class I maser transitions are the $7_0 - 6_1 A^+$ transition at 44 GHz, $4_{-1} - 3_0 E$ transition at 36 GHz, $5_{-1} - 4_0 E$ transition at 84 GHz, $6_{-1} - 5_0 E$ at 132 GHz, $8_0 - 7_1 A^+$ transition at 95 GHz etc., while Class II transitions are the $5_1 - 6_0 A^+$ transition at 6.7 GHz, $2_0 - 3_{-1} E$ transition at 12 GHz, the series of $J_0 - J_{-1} E$ transitions at 157 GHz, etc. The strongest Class I masers (usually called MMIs) emit at 44 GHz and demonstrate flux densities up to 800 Jy (Haschick et al. 1990), while the strongest Class II masers (MMII) emit at 6.7 GHz and some of these achieve flux densities of ~ 4000 Jy (Menten, 1991a). Here we consider only MMIs; for a more thorough description of their main properties see the contribution by Leurini & Menten (this volume).

Until recently it was considered that methanol masers arise only in massive star for-

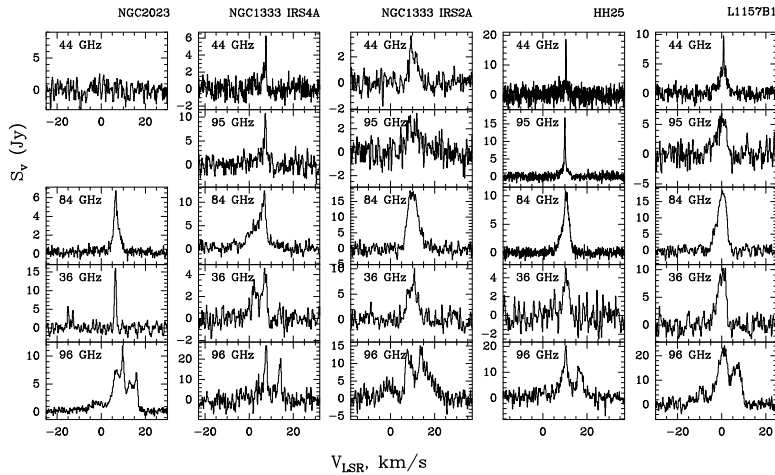


Figure 1. LMMI spectra at 44, 95, 84, and 36 GHz, taken at the Onsala Space Observatory. Purely thermal $2_K - 1_K$ methanol lines at 96 GHz are shown in the bottom row.

mation regions (MSFRs). But in the past few years several MMIs have been found in nearby low-mass star formation regions (LMSFRs) NGC1333, NGC2023, HH25, and L1157 (Kalenskii et al. 2006, Kalenskii et al. 2010a, Kang et al. 2013, Lyo et al. 2014). The masers were detected in the Class I lines at 36 GHz, 44 GHz, 95 GHz, and 132 GHz.

2. LMMI properties

MMIs in LMSFRs (hereafter called LMMIs) have been studied using the 20-m Onsala radio telescope and the KVN 21-m telescopes in a single-dish mode (Kalenskii et al. 2010a, Kang et al. 2013, Lyo et al. 2014). In addition, four objects have been observed at 44 GHz with the VLA in the D configuration (Kalenskii et al. 2010b, Kalenskii et al. 2013) with a spatial resolution of $\sim 1.5''$. The spectra of the lines observed at Onsala are shown in Fig. 1. The main LMMI properties are discussed in Kalenskii et al. (2013). They can be summarised as follows:

- All known LMMIs are associated with chemically active bipolar outflows, where the gas-phase abundance of methanol is enhanced due to grain mantle evaporation. VLA observations show that LMMIs are related to the shocked gas in the outflow lobes.
- The known LMMIs are associated with clouds where the column densities of methanol are no less than 10^{14} cm^{-2} . Kalenskii et al. (2010a) suggested that MMIs can arise only when methanol column density is above this value.
- Flux densities of LMMIs do not exceed 18 Jy at 44 GHz and are lower in the other Class I lines (see Fig 1). However, LMMI luminosities at 44 GHz match the relation between the protostar and maser luminosities $L_{\text{CH}_3\text{OH}} = 1.71 \times 10^{-10} (L_{\text{bol}})^{1.22}$, established for high- and intermediate-mass protostars by Bae et al. (2011).
- No variability at 44 GHz was detected in NGC1333I4A, HH25, or L1157 during the time period 2004–2011.
- Radial velocities of most LMMIs are close to the systemic velocities of associated regions. The only known exception is the maser detected at 36 GHz toward the blue lobe of the extra-high-velocity outflow in NGC 2023, whose radial velocity is 3.5 km s^{-1} lower than the systemic velocity.

Thus, one can see that the main properties of LMMIs are similar to those of HMMIs. LMMIs are likely to be a low luminosity edge of the overall MMI population. Therefore

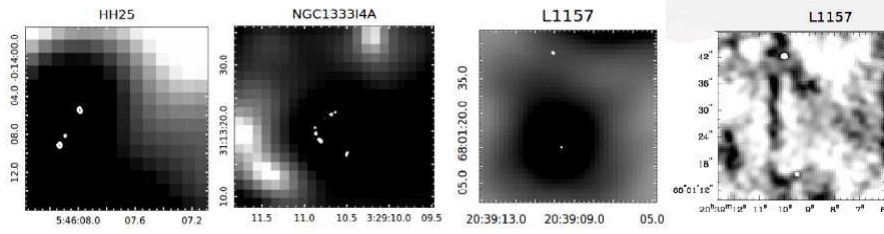


Figure 2. Three left panels: EVLA maps of methanol masers at 44 GHz (white dots) overlaid upon W1 (HH25 and NGC1333I4A) and W4 (L1157) WISE images. Right panel: methanol masers overlaid upon the map of the $5_0 - 4_0A^+$ thermal emission in L1157.

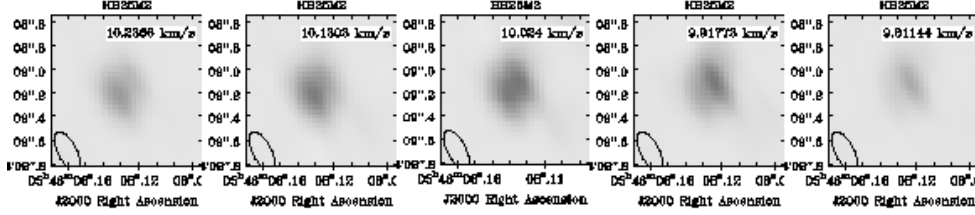


Figure 3. Example of a double spot: channel map of HH25M2 at 44 GHz.

the question arises, why should we study these few weak objects instead of focusing on much stronger MMIs in MSFRs? The answer is that the study of Class I methanol masers in LMSFRs might be more straightforward compared to the study of the "classical" MMIs in MSFRs, because, in contrast to MSFRs, LMSFRs are widespread and many of them are located only 200–300 pc from the Sun; they are less heavily obscured in optical and IR wave ranges, and there are many isolated low-mass Young Stellar Objects (YSOs). We continue to study MMIs in LMSFRs in order to better understand Class I methanol masers. Here we present the results of the observations of three maser sources performed at 44 GHz with the EVLA in the B configuration as well as CARMA observations of L1157 in the thermal lines of methanol $5_K - 4_K$ at 241 GHz.

3. New results

Spatial resolution of about $1.5''$, achievable at 44 GHz with the VLA in the D configuration, proved to be insufficient to resolve individual maser spots and measure their sizes and brightness temperatures. Therefore in 2013 we reobserved three LMMIs, HH25, NGC1333I4A, and L1157 at 44 GHz using EVLA in the B configuration, which provides an angular resolution of about $0.2''$ at 44 GHz. In addition, we observed L1157 in the $5_K - 4_K$ thermal lines of methanol at 241 GHz with the antenna array CARMA in the C configuration with an angular resolution of $\approx 1''$.

A collection of the overall maps of the three observed sources at 44 GHz is shown in Fig. 2. The maps show that each source consists of several spots. Hereafter M1 means the strongest spot in the region, M2 is the second strongest spot etc. Deconvolved spot sizes vary from $\sim 0.10''$ – $0.15''$ for the stronger spots to $\sim 0.10''$ – $0.3''$ for the weaker spots (30–45 AU and 30–90 AU, respectively).

The brightness temperatures of the strongest spots are as high as 5×10^5 K.

Maser spots in NGC1333I4A form an arc around a NIR object clearly seen in the W1 and W2 WISE maps.

The maps of individual spots show that many of them can be decomposed into two un-

resolved compact subspots. In these cases the brightest subspot is denoted subspot a, the second brightest subspot, subspot b. An example of such double spot is shown in Fig. 3, which exhibits the channel map of the second brightest spot in HH25 (HH25M2). Among the spots that demonstrate double structures are L1157M1 and M2, NGC1333I4AM2 etc.

An interesting result is the detection of unresolved spots demonstrating broad ($\gtrsim 3 - 5 \text{ km s}^{-1}$) spectral lines. Their fluxes are about 0.1–0.2 Jy, which corresponds to brightness temperatures $\gtrsim 1000 \text{ K}$. Thus, in spite of large linewidths, these objects are probably weak masers.

4. Discussion

According to the most popular maser model, compact maser spots arise in extended turbulent clumps because in a turbulent velocity field the coherence lengths l along some lines are increased. If masers are associated with turbulence, the map appearance depends on the maser regime. Saturated regime of maser amplification is characterized by a large number of spots of comparable intensity, while the unsaturated maser amplification results in a small number of bright spots (Strel'nitski et al. 2017). The map of maser emission in L1157 with only two maser spots (Fig. 2) favors the unsaturated regime of maser amplification, which was studied by Sobolev et al. (1998).

One of the main parameters of the model by Sobolev et al. is τ_0 , the absolute value of optical depth at the center of the inverted line when there is no turbulence in the cloud. From the intensities of thermal lines $5_K - 4_K A^+$ toward M1, observed with CARMA, we estimated $N_{\text{CH}_3\text{OH}}$ ($\sim 10^{16} \text{ cm}^{-2}$) and τ_0 at 44 GHz (~ 12). From Table 1 of Sobolev et al. (1998) we estimated that the optical depth at 44 GHz toward M1 is $\tau^{44} \sim 7 - 8$ and T_{br} at this frequency $\sim 10^4 \text{ K}$, much lower than the observed one. However, an increase of $N_{\text{CH}_3\text{OH}}$ by a factor of less than 2 makes it possible to achieve the observed brightness temperature. Thus, the turbulence model is in "marginal" agreement with the observations.

SVK acknowledges the support of the Russian Foundation for Basic Research (project no. 15-02-07676).

References

- Bae J.-H., Kim, K.-T., Youn S.-Y., Kim W.-J., Byun D.-Y., Kang H., & Oh C. S. 2011, *ApJS* 196, 21
- Haschick A. D., Menten K. M., & Baan W. 1990, *ApJ* 354, 556
- Kalenskii S. V., Promyslov V. G., Slysh V. I., Bergman P., & Winnberg A. 2006, *Astron. Rep.* 50, 289
- Kalenskii S.V., Johansson L.E.B., Bergman P., Kurtz S., Hofner P., Walmsley C.M., & Slysh V.I. 2010a, *MNRAS* 405, 613
- Kalenskii S.V., Kurtz S., Slysh V.I., Hofner P., Walmsley C.M., Johansson L.E.B., & Bergman P. 2010b, *Astron. Rep.* 54, 932
- Kalenskii S.V., Kurtz S., & Bergman P. 2013, *Astron. Rep.* 57, 120
- Kang M., Lee J.-E., Choi M., Choi Y., Kim K.-T., Di Francesco J., & Park Y.-S. 2013, *ApJS* 209, 25
- Lyo, A.-R., Kim, J., Byun, D.-Y., & Lee, H.-G. 2014, *AJ* 148, 80
- Menten K.M. 1991a, *ApJ* 380, L75
- Menten, K.M. 1991b, *ASP Conference Series*, 16, 119
- Sobolev, A.M., Vallin, B.K., & Watson, W.D. 1998, *ApJ* 498, 763
- Strel'nitski, V.S., Holder, B.P., Shishov, V.I., & Nezhdanova, N.I. 2017, *Astron. Astrophys Trans-actions*, in press